APPLIED RESEARCH

Design of an Asymmetric Damping Structure for a Single Cylinder and Single Rod MR Damper

JIANGQI LONG[ID]**¹, MIN ZHOU¹, YINGHAO HU¹, AND JIANHONG ZHANG²**

¹School of Mechanical Electrical Engineering, Wenzhou University, Wenzhou 325035, China
²Zhejiang Sensen Auto Parts Ltd., Wenzhou 325204, China

Corresponding author: Jiangqi Long (longjiangqi@163.com)

ABSTRACT Magnetorheological (MR) dampers possess the ability to alter the damping force of the damper by modifying the viscosity of Magnetorheological Fluid (MRF). The prevalent MR dampers mostly feature a single damping channel structure, which necessitates adjusting the magnetic field strength to attain asymmetric damping force during the compression and recovery stroke. However, it amplifies the influence of the control circuit's time-delay on damping force. This article proposes the design of a dual-damping-channel MR damper to structurally achieve the asymmetric damping force. The dimensions of key components were determined using damping calculation formulas and electromagnetic simulation. A prototype MR damper was manufactured, and experimental verification was conducted. The results indicate that the damper operates optimally, and the damping force value and adjustable range of damping force meet the design objectives. The indicator characteristic curve of the shock absorber shows that the MR shock absorber designed in this paper can effectively reduce the influence of MRF time-delay on the damping force value of the shock absorber.

INDEX TERMS Asymmetric damping characteristics, dual-damping-channels, electromagnetic simulation, MR damper, time-delay.

I. INTRODUCTION

A damper with a smaller damping coefficient has the ability to release the vibration generated by the tires in a smoother manner, thereby enhancing the riding comfort of the car. Conversely, a large damping damper has the capability of absorbing the potential energy more efficiently, thereby enhancing the vehicle's handling stability [1]. The fixed damping of conventional dampers can only fulfill the requirements of riding comfort and operational stability under certain fixed working conditions. The magnetic rheological (MR) damper with adjustable damping, on the other hand, has the ability to balance the riding comfort and handling stability of cars under various working conditions, and has recently become a focal point of suspension research [2].

Lord Company [3] has designed and prepared three types of MR damper structures with double cylinders and a single

The associate editor coordinating the review of this manuscript and approving it for publication was Xiaojie Su[ID].

output rod. In the current research on MR dampers, the primary design objective is often to increase the adjustable range of damping force [4], prevent MRF settlement [5], reduce development costs [6], [7], and improve energy utilization efficiency [8], etc. To ensure driving safety and comfort, it is essential that the recovery damping coefficient of the damper is greater than the compression damping coefficient [9]. Existing MR dampers typically have equal damping coefficients during compression and restoration processes. Asymmetric damping characteristics are achieved by adjusting the magnetic field strength. However, this approach requires highly accurate displacement sensors and efficient control circuits. This drawback would amplify the time-delay issue of MR dampers, resulting in a suboptimal driving experience [10]. Govinda et al. concluded, through simulation comparisons, that the Bouc-Wen model is more suitable for describing the damping force delay caused by the state change of MRF in MR dampers [11]. Additionally, Bogdan et al. developed a nonparametric control circuit

model for MR dampers using the support vector method. This model accurately predicts the response to current excitation [12]. Xie et al. proposed a programmable high-speed and low-cost current source specifically for MR Damper, which has a very stable high-speed response and effectively reduces the time-delay effect caused by power excitation [13]. In order to realize the precise control of hydraulic lifting system, Liu et al. proposed a magneto-rheological valve structure with mixed magnetic supply sources. Through experiments, it was found that the rise response time performance increased with the increase of current, but the response time performance decreased without the influence of current [14]. These studies contribute to the ongoing advancement of MR dampers and pave the way for further improvements in their performance and applicability.

To mitigate the time-delay effect of MR dampers, minimize the quantity of damper sensors, and simplify control strategies, this article presents a design for a dual-damping-channel MR damper with asymmetrical damping properties. Structurally, the asymmetric damping characteristics of the MR damper were achieved, which were further verified through experimentation using a prototype. By contrasting the experimental outcomes against the design objectives, the accuracy of the theoretical calculations and electromagnetic simulations employed in the design process was demonstrated. Furthermore, a comparison of the damper's time-delay characteristics confirms the efficacy of the MR damper structure proposed in this article for mitigating the impact of damping force time-delay.

II. STRUCTURAL DESIGN OF MR DAMPER

A. THE TIME-DELAY CHARACTERISTICS OF THE MR DAMPER

The time-delay characteristics of the MR damper refer to the inherent lagging phenomenon in the suspension control system, including the data acquisition time of the vehicle state sensor, the computation time for the suspension system vibration control signal, and the response time of the actuator [15]. These time delays in the MR damper can result in a deterioration of ride comfort. In traditional dampers, the damping channels are equipped with valve plate stiffness adjustments at both ends, enabling the recovery damping coefficient to be greater than the compression damping coefficient, as shown in Fig. 1.

The high viscosity and density of magneto-rheological (MR) fluid can generate significant zero-field damping force (damping force without applying electrical excitation) when flow is controlled by valve plates. Existing MR dampers commonly use open damping channels to achieve a normal range of zero-field damping force. Hu et al. invented a high-speed shock absorber for rotary mixing MR Fluid, which can make magnetic particles uniformly distributed in MR Fluid [16]. Deng et al. invented a multi-magnetic circuit shock absorber with permanent magnets. The coil is placed outside, and the design structure is simple, which can effectively reduce the
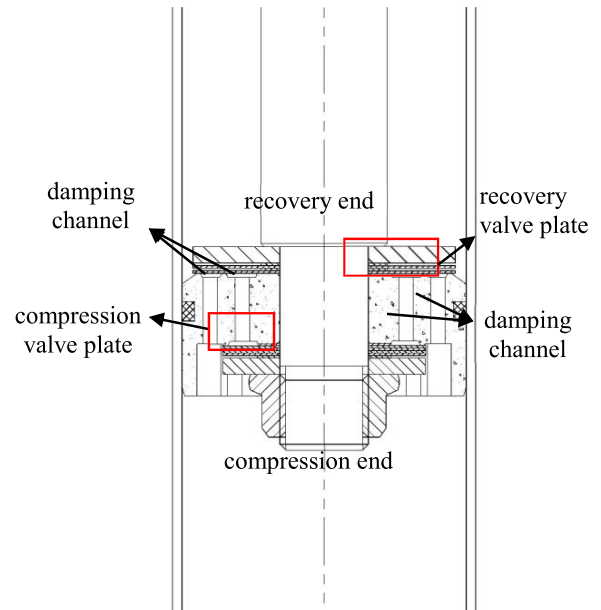

FIGURE 1. The damping structure of traditional damper.

cost [17]. Liu et al. invented a new type of magnetorheological elastomer shock absorber, which has high control precision and sensitive response [18]. Zhu et al. invented a new type of piston internal flow channel magnetorheological shock absorber, which can accurately adjust the vibration generated by the vehicle, and has stable work and high efficiency. It can effectively prevent damping hardening [19]. However, the above designed MR Damper does not consider the influence of time delay.

The damping coefficient of the damping channel is related to the viscosity of the magneto-rheological fluid and the diameter of the damping channel. The diameter of the damping channel is fixed and can only be adjusted at the moment of switching between compression and recovery strokes (When the piston reaches the upper/lower end position, it means that the piston velocity is changing from positive to negative or from negative to positive, as shown in Fig. 2) to control the magnitude of the magnetic field strength and achieve the goal of the recovery damping coefficient being greater than the compression damping coefficient. This method easily amplifies the hysteresis disadvantage of the MR damper when the piston is moving at high speed. Under the same time delay, the higher the piston velocity, the larger the time delay displacement caused by the time delay. In addition, the faster the piston velocity, the shorter the position of staying at the upper and lower dead points, making it more difficult to capture the timing of magnetic field adjustment, and more prone to errors.

A dual-damping channel magnetorheological (MR) damper is designed in this study, where the valve disc, claw spring, and damping channels are coordinated. It does not require complex control strategies, and a under constant magnetic field intensity, it achieves asymmetric damping characteristics during compression and recovery strokes.
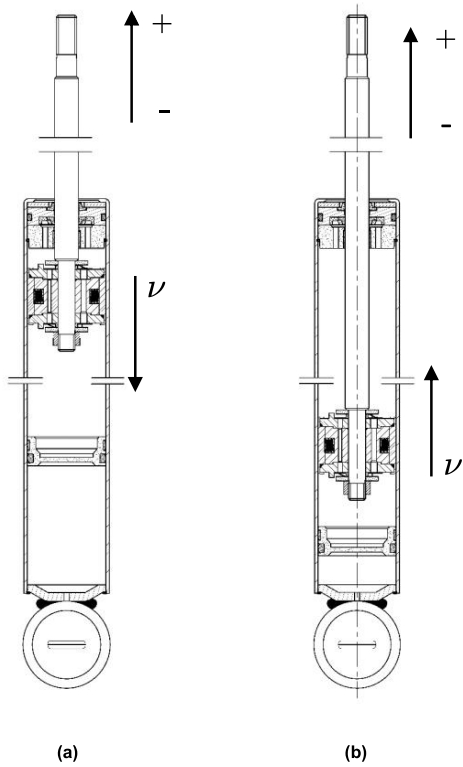
(a)   **(b)**

FIGURE 2. Damping piston upper (a) and lower (b) end stops.

B. DAMPING SYSTEM DESIGN OBJECTIVES AND RESULTS

The prototype of MR Damper designed in this paper is based on the front damper of a Dongfeng vehicle. The performance requirements for this prototype are detailed in Table 1.

TABLE 1. Design objectives of MR dampers.

Object	Value	Object	Value
Maximum recovery damping force	2000 N	Adjustable range of recovering damping force	>500 N
Maximum compression damping force	1000 N	Adjustable range of compression damping force	<100 N
Current excitation	0-2 A	MRF model	A172-P0202206

Note: Both the maximum compression and maximum recovery damping forces are measured when the current excitation is 0 and the piston velocity is 0.52 m/s.

Currently, there are two primary structural forms of MR dampers: double-cylinder and single-cylinder. The double-cylinder damper structure is relatively complex, and the bottom valve is prone to blockage, making it difficult to recover the damping force after long periods of disuse [20]. Single-cylinder dampers come with two structural forms: single outcome rod and double outcome rod. However, considering that the double extension rod takes up a large amount of space, it's not suitable for the use of car suspension system which has limited space [21]. To meet the design objectives,

this article proposes a dual-channel damper with asymmetric damping characteristics, which is primarily composed of a piston rod, piston rod sealing component, guide ring, working cylinder, piston component, floating piston, bottom cover, lifting ring. The structural assembly of the damper is illustrated in Fig. 3.

In order to meet the design objectives proposed in this paper and assemble with the reference model, the outer diameter, inner diameter, and length of the working cylinder of the shock absorber are designed to be 50 mm, 46 mm, and 330 mm, respectively. The working cylinder strength verification formula is as follows:

$$D \geq \sqrt{\frac{4F_{max}}{\pi [p] (1 - \lambda)^2}} \tag{1}$$

where $[p]$ is the maximum allowable pressure in the cylinder, taking 4 N/mm^2; F_{max} is 2306.6 N for the maximum output force of the shock absorber; λ is the ratio of the piston rod of the shock absorber to the diameter of the working cylinder, of which, the single cylinder shock absorber is generally 0.3-0.35, here 0.35 is taken, and $D \geq 41.6867$ mm is calculated, and the designed working cylinder meets the requirements.

The piston rod diameter of the single cylinder shock absorber is generally 0.3-0.35 times that of the working cylinder. Therefore, the designed piston rod range should be 13.8-16.1 mm. The diameter of the piston rod designed in this paper is 14 mm, and its length is 360 mm. The tensile strength of the piston rod is verified:

$$\sigma_{max} = \frac{4F_{max}S}{\pi D_1^2} = 44.9518Mpa \leq [\sigma] = 180Mpa \tag{2}$$

where $[\sigma]$ is the allowable stress of 45 steel; S is the safety factor of 3.

During the process of compression, which is responsible for compressing blocks into three smaller entrances, while the MRF enters the damping channels through the larger diameter entrance. The outlet of the small damping channels is obstructed by the recovery valve plate. However, due to the pressure generated by the flow of MRF, the claw spring at the end of the compressed recovery valve plate contracts, thus pushing the recovery valve plate open. The MRF then flows out from the gap between the flow valve stopper and the recovery valve plate, successfully compressing the stroke MRF through three small damping channels. Fig. 4 (a) depicts the compression end of the piston assembly. Similarly, the objective of recovering the stroke MRF to flow through three damping channels with a smaller diameter is attained using the same method. Fig. 4 (b) illustrates the recovery end of the piston component.

The damping device designed in this study, without major modifications to the piston components, only incorporates valve plates and a pawl spring structure, which is coordinated with the damping channel to achieve the asymmetry of compression and recover damping forces. In addition, the designed damping device has the advantages of a simple structure and adjustable parameters. This indicates that the
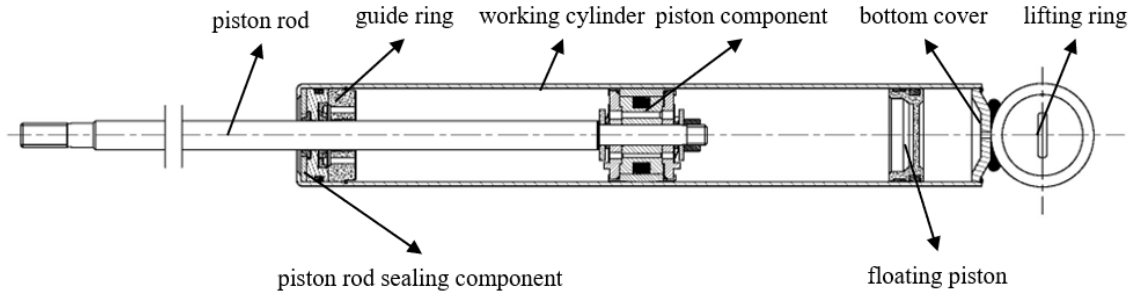
piston rod   guide ring   working cylinder piston component   bottom cover   lifting ring

piston rod sealing component

floating piston

FIGURE 3. General assembly structure of MR damper.

compression valve plate

claw spring

(a)

smaller diameter entrance

claw spring

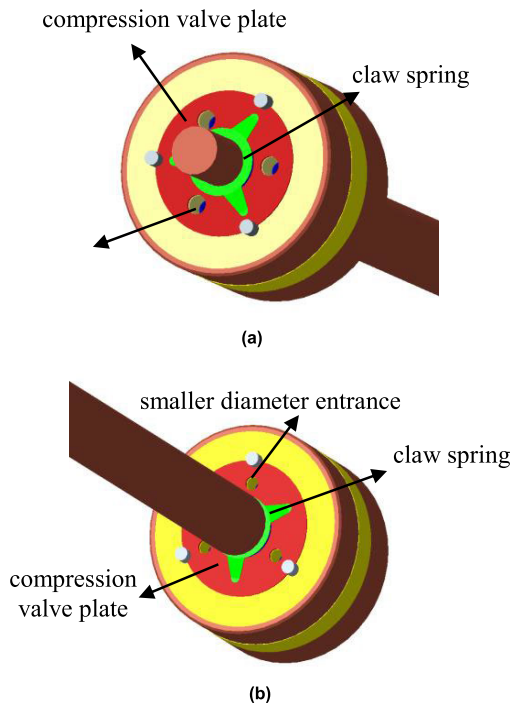compression valve plate

(b)

FIGURE 4. Schematic diagram of piston component structure (a) compression end and (b) recovery end.

damping device structure has strong plasticity. By changing parameters such as the pawl spring stiffness, magnetorheological fluid density, and damping channel diameter, the basic damping force and adjustable range of damping force of the damping device can be adjusted to meet different working conditions.

III. MECHANICAL CHARACTERISTICS ANALYSIS OF DAMPERS

The total damping force of the MR damper can be expressed as [22]:

$$F = F_v + F_{MR} + F_a + F_f \tag{3}$$

where F is the total damping force; F_v is the viscous damping force; F_{MR} is the shear damping force caused by the magnetorheological effect; F_a is the gas rebuttal force caused by the floating piston; F_f is the frictional damping force.

In the MR damper structure presented in this article, the main component of F_f is the frictional damping force between the piston ring and the working cylinder. This force is relatively small and can be disregarded. On the other hand, the magnitude of the gas rebuttal force F_a is dependent on the size of the piston rod's volume and the diameter of the working cylinder. To obtain this force value of the damper, a damper with the same dimensions of the piston rod and working cylinder as the design structure was employed for performance experiment. The gas rebuttal force value obtained from this experiment was 306.6 N. According to Table 1, the recovery damping force is $F_v = 2306.6$ N.

A. VISCOUS DAMPING FORCE

The viscous damping force is primarily correlated with the pressure drop at both ends of the damping channel and the effective area of the piston. The specific relationship can be expressed as [23]:

$$F_v = \Delta P_v A_p \tag{4}$$

$$\Delta P_v = \rho g h_f = f \frac{\rho L V_d}{2 D_h} \tag{5}$$

$$V_d = \frac{A_p V_p}{A_d}, D_h = d \tag{6}$$

where ΔP_v is the pressure drop due to viscous damping, A_P is the effective area of the piston, ρ is the density of MRF, g is gravitational acceleration, h_f is the height difference of viscous resistance, f is the Darcy friction factor, L is the length of the damping channel, V_d is the average flow velocity of MRF in the damping channel, V_P is the piston motion speed, A_d is the damping channel cross-sectional area, D_h is the hydraulic diameter, and d is the diameter of the damping channel. It is worth noting that there are 3 compression and recovery damping holes each.

In the MR damper structure designed in this article, L represents the height of the piston body and has a value of 22 mm. The MRF material used in this study has properties as follows: $\rho = 2.33 \times 10^{-9}$ ton/mm^3, and $V_P = 520$ mm/s. Since the damping channel diameters for compression and recovery are different, V_P is discussed separately for each stroke. The effective area of the piston in the compression stroke is

given by:

$$A_p = \pi \left(R^2 - r^2 - \frac{d_1}{4} \times 3 \right) \quad (7)$$

A_P in the recovery stroke is:

$$A_p = \pi \left(R^2 - r^2 - \frac{d_2}{4} \times 3 \right) \quad (8)$$

where R represents the piston radius, r represents the radius of the piston rod, and d_1 and d_2 represent the diameters of the damping channels for the compression and recovery strokes, respectively. The geometric parameter relationships in equations (6), (7), and (8) are depicted in Fig. 5.
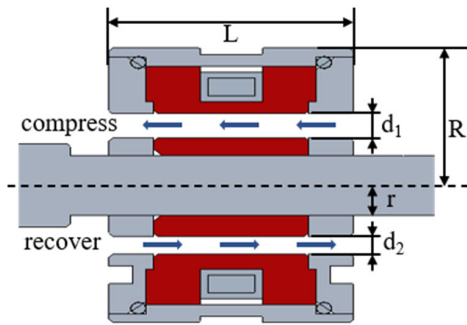

FIGURE 5. Schematic diagram of piston structure fluid circuit.

f is determined by Reynolds number segments [24]:

$$f = \begin{cases} \dfrac{96}{\text{Re}} & \text{if } \text{Re} \leq 2000 \\[2mm] (1-\alpha)\dfrac{96}{2000} + \alpha \dfrac{1}{\left\{ 1.8 \log_{10}\left[\left(\frac{\varepsilon/D_h}{3.7}\right)^{1.11} + \frac{6.9}{4000} \right] \right\}^2} \\[2mm] \qquad \text{if } 2000 < \text{Re} \leq 4000 \\[2mm] \dfrac{1}{\left\{ 1.8 \log_{10}\left[\left(\frac{\varepsilon/D_h}{3.7}\right)^{1.11} + \frac{6.9}{\text{Re}} \right] \right\}^2} & \text{if } \text{Re} \geq 4000 \end{cases}$$

$$(9)$$

where ε is the average roughness of the pipe wall, α can be expressed as:

$$\alpha = \frac{Re - 2000}{4000 - 2000} \quad (10)$$

Reynolds number is defined as [25]:

$$Re = \frac{\rho V_d D_h}{\eta} \quad (11)$$

where η is the dynamic viscosity of MRF material, and in this article, η is taken as 1.01×10^{-6} MPa·s [26].

The existing parameters such as ρ, L, η, and V_P can be obtained by plugging them into Equations (6)-(8) and (11):

$$Re = \frac{\rho V_d D_h}{\eta} = 2.3 \times 10^{-2} \times \frac{480 - 0.75 d^2}{d} \quad (12)$$

The design of damping channels takes a diameter ranging from 1 to 5 mm. When $d = 1$ mm, however, the Reynolds number has a maximum value of $Re = 11.04$, which is less than 2000. By combining equations (4)-(9) and according to $F_v = 2306.6$ N, we can conclude that $d = 3.22$ mm. Considering the pretension of the claw spring in the shock absorber and the disturbing effect of the limit block, the diameter for the recovery damping is chosen to be 3.5 mm.

Similarly, the compression damping diameter is calculated to be 3.87 mm. Considering the pretension of the jaw spring and the disturbance and current limiting effect of the limit block, and according to the design and test experience of the engineer, when $d \geq 4$ mm, the magneto rheological effect of the compression process is not obvious, and the diameter of the compression damping hole is 4 mm.

B. SHEAR DAMPING FORCE

The shear damping force is generated by the magnetorheological effect of the MRF, and its magnitude can be expressed as [25]:

$$F_{MR} = \Delta P_{MR} A_P \text{sgn}(V_P) \quad (13)$$

$$\Delta P_{MR} = \frac{L\tau}{D_h} \quad (14)$$

where τ is the shear stress of the MRF.

In this paper, micron-level MRF material with fine soft magnetic particles is selected, and the product batch is A172-P0202206. The basic properties of the material are shown in the table.

TABLE 2. Basic performance of MRF products.

Product batch	Test name	Magnetic particle content	MR Fluid density	Resistance to settlement
A172-P0202206	Reference index	≥72%	2.30~2.45 g/cm³	Settlement rate within 7 days at 25 °C≤3.2%
	Practical measured value	72%	2.33 g/cm³	Settlement rate within 7 days at 25 °C is 2.73%

The H-τ curve and H-B curve of the MRF material were obtained from the mechanical property test, and the relationship curve between shear stress and magnetic induction intensity was obtained by sorting out the relevant data and fitting, as shown in Fig. 6.

As illustrated by the B-τ relationship curve in Fig. 6, the growth trend of MRF shear stress slows down significantly after the magnetic induction intensity reaches 0.776 T, with the corresponding shear stress measured to be 43.44 kPa. Upon reaching 1 T, the shear stress approaches saturation at 47.69 kPa. Under ideal conditions, the maximum shear damping force of the MR damper is achieved when the magnetic induction intensity reaches 1 T. Substituting parameters τ and D_h into equations (13) and (14), where $F_{MR} = 636.54$ N, the maximum magnetic induction intensity is set between 0.776-1 T, based on the variation of MRF shear stress
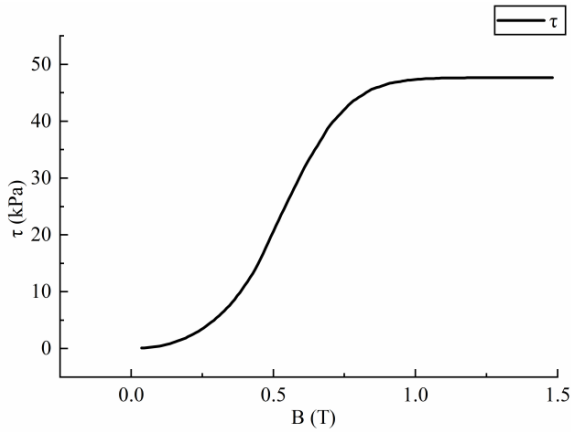
FIGURE 6. B-τ relationship curve.

with magnetic induction intensity, in order to meet the design target.

IV. ELECTROMAGNETIC SIMULATION ANALYSIS

In this article, Maxwell software was used to perform an electromagnetic simulation of the MR piston structure, and the parameters of the energized coil were determined based on the simulation results. The majority of the relative permeability values for materials in the Maxwell material library are fixed. However, the magnetic induction intensity in the iron core will increase linearly with the increase of magnetic induction intensity in the energized coil and will not approach magnetic saturation. This is not sufficient to meet the accuracy requirements for quantitative analysis. In this paper, the relative permeability of two key materials in the electromagnetic simulation, the piston main materials DT4C and MRF, are treated nonlinearly. Based on the results of the electromagnetic performance experiment, the relative permeabilities of the materials were obtained, and the magnetization curves of DT4C and MRF materials are presented in Fig. 7.

Other parts, such as copper coil, flow valve limiter, and piston sleeve steel, have specific relative magnetic permeability parameters shown in the table below.

TABLE 3. Materials and relative magnetic permeability of each part.

Parts name	Piston bush	Coil	The rest part
Material	Steel	Copper	Air
Relative magnetic permeability	400	1	1

An analysis domain of finite volume was generated at 20 times the maximum size of the model in the xyz direction, and the creation result of the analysis domain is shown in Fig. 8. The magenta cuboid part in the figure is the created analysis domain.

In this paper, only the ampere-turns of the coil are used in the simulation calculation. The current excitation is added to the section, and the twisted coil type excitation is selected.
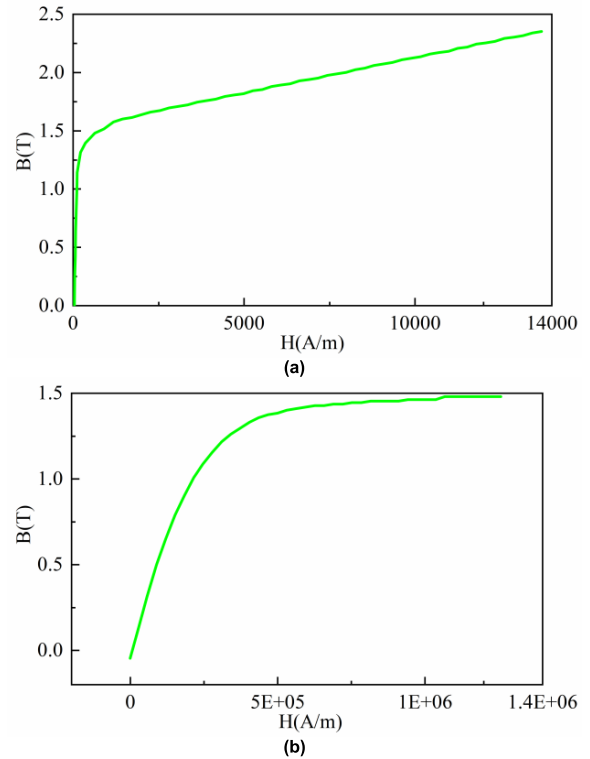

FIGURE 7. Material magnetization curve (a) DT4C and (b) MRF.
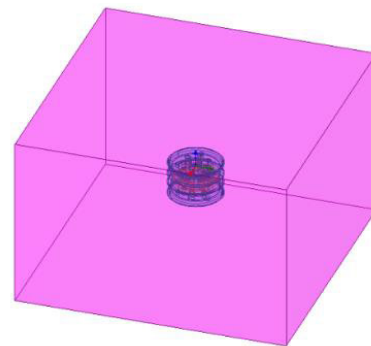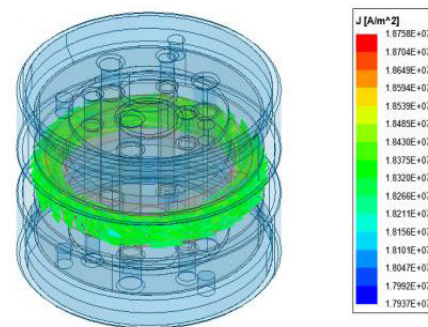

FIGURE 8. 3D simulation analysis domain.

FIGURE 9. Excitation current density vector diagram.

The figure shows the current density vector diagram generated after inputting 400 A ampere-turns excitation.

In this paper, the piston body and the flow valve limiter are irregular parts. In order to verify mesh independence, the 8 mm, 5 mm, and 3 mm mesh are used for simulation analysis respectively. It is found that with the decrease of the mesh size, the influence on the final parameter change is very small, indicating that the simulation results are not sensitive to the mesh. A 5 mm mesh was used as the final mesh division scheme. After finishing the simulation calculation, the scalar and vector results of magnetic induction intensity of the main part of the piston under the current excitation of 400 A ampere-turns are shown in Fig. 10.
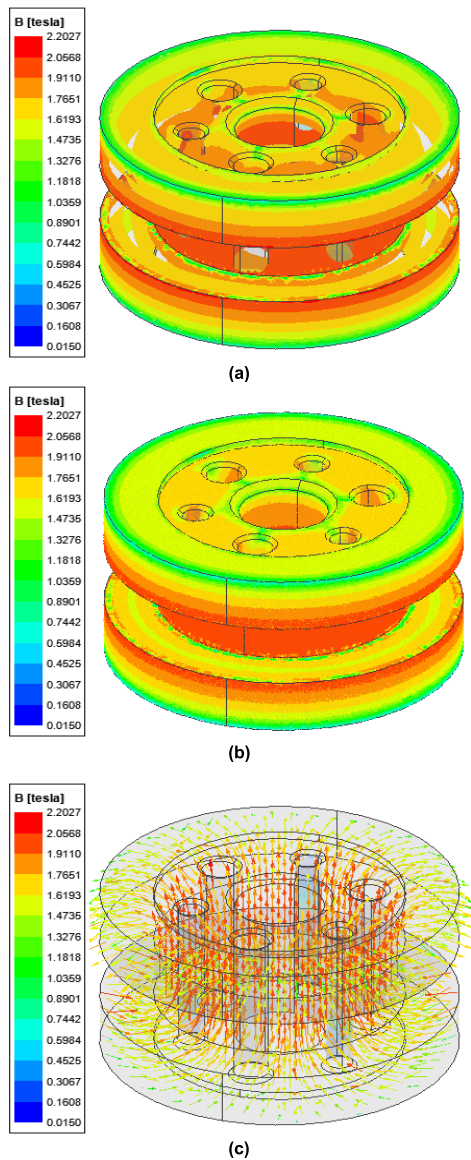
(a)

(b)

(c)

FIGURE 10. Simulation results of magnetic induction intensity of main body (a) Isosurface, (b) Cloud map, and (c) Vector map.

(a)

(b)

(c)

(d)

FIGURE 11. Magnetic induction intensity simulation results: (a) 100 A, (b) 200 A, (c) 300 A, and (d) 400 A.

The magnetic induction intensity simulation results under each excitation were sorted out, as presented in Fig.11. For an excitation of 100 A, the maximum magnetic induction inte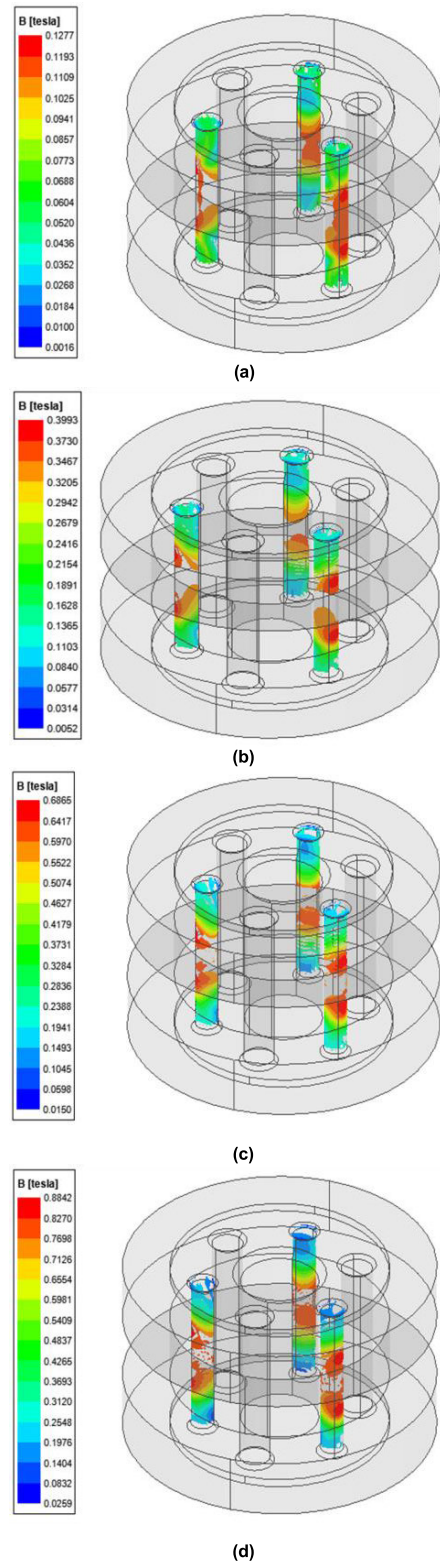nsity in the damping channel is situated in the middle section of the damping channel, with a value of 0.1277 T. For an excitation of 200 A, the maximum magnetic induction

intensity in the damping channel is 0.3993 T at the middle upper part and middle lower part of damping channel, respectively. For an excitation of 300 A, the maximum magnetic induction intensity in the damping channel is located at the middle upper part and middle lower part of damping channel, with a value of 0.6865 T. Lastly, for an excitation of 400A, the maximum magnetic induction intensity in the damping channel is situated at the upper and lower end faces of the corresponding coil grooves of the MRF, with a value of 0.8842 T. This value falls within the range of 0.776-1 T magnetic induction intensity, thus meeting the design goal. Based on the electromagnetic simulation results, the number of turns for the excitation coil was determined to be 200, and the maximum current was 2 A.

The coil is arranged in the middle position of the piston body, using enameled copper wire. Each turn of the coil is insulated from each other, and the diameter of the wire is 0.3 mm. The position of the coils in the piston component can be seen in Fig. 12.
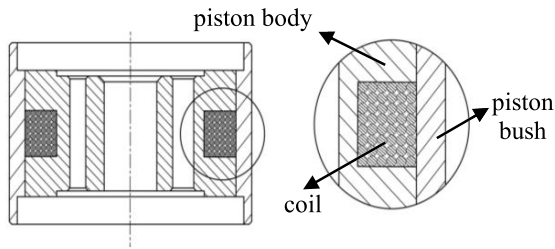

FIGURE 12. The schematic diagram illustrating the arrangement of coils. Note: The coil section shown in the diagram is only representative of the coil placement area and does not correspond to the actual number of coils.

In order to more clearly represent the magnetic field distribution in the piston, an excitation of 200 turns 2 A was input at the coil position, and two-dimensional electromagnetic simulation was carried out on part of the piston cross-section. The electromagnetic simulation results are shown in Fig. 13. It can be seen from the figure that the magnetic induction line at the convex head of the upper and lower ends of the coil groove is wrapped into the piston sleeve part, and the
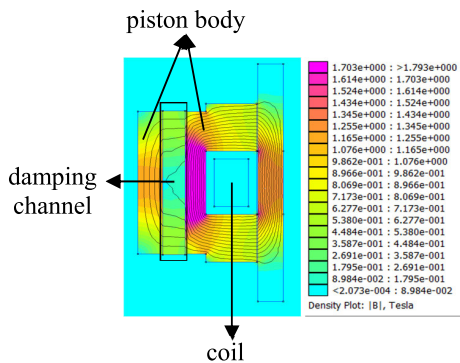

FIGURE 13. Magnetic induction intensity simulation results. Note: The black curves represent magnetic field lines.

overall magnetic induction intensity of the component is high. The maximum magnetic induction intensity is located in the middle of the coil groove, which is 1.703 T. The magnetic induction intensity at MRF is 0.8069 T, which is still within the range of 0.766-1 T required by the design target.

V. PROTOTYPE TRIAL PRODUCTION AND EXPERIMENT
A. PROTOTYPE TRIAL PRODUCTION
The key components of the MR damper structure designed in this article are non-standard parts that require independent processing. The primary processes used include turning, grinding, wire cutting, drilling, etc. The processed parts are assembled with standard components such as guide sleeves, piston rod sealing rings, and floating pistons according to the design concept, as depicted in Fig. 14. Fig. 14 (a) displays the assembly of the internal piston components, mating parts, and piston rods of the damper. Subsequently, the completed piston rod assembly was installed into the working cylinder, and the specific process was as follows: MRF was poured into the working cylinder → the piston component part was installed in the piston rod assembly → the snap ring was installed inside the upper end of the working cylinder, as shown in Fig. 14 (b) → the guide seat was pressed in → the sealing ring was tightly pressed in. The snap ring set at the guide sleeve on the inner wall of the working cylinder was employed to prevent the guide sleeve and piston rod sealing ring from being pressed into the inner part of the working cylinder. The physical image of the MR damper assembly after installation is presented in Fig. 14 (c).
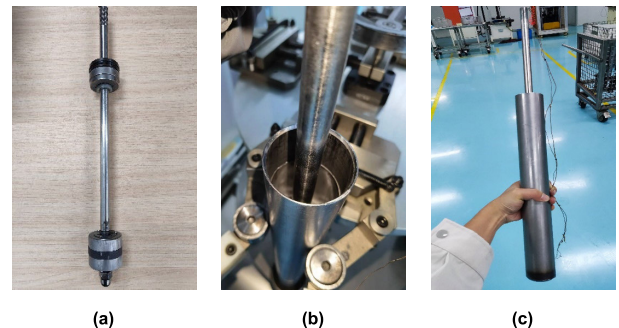

(a)   (b)   (c)

FIGURE 14. Assembly of MR damper components (a) Installation of internal components, (b) Installation of snap rings, and (c) Damper assembly.

In order to verify that the magnetic induction intensity in the damping channel of the piston assembly designed meets the design goal, the excitation currents of 0.5 A, 1 A, 1.5 A, and 2 A are respectively input. The Tesla meter (as shown in Fig. 15) is used for multiple measurements, and the average value is taken. Under different current excitations, the magnetic induction intensity in the damping channel is shown in Table 4.

It can be seen from the table that under different current excitations, the magnetic induction intensity at the damping channel is consistent with the simulation results. When the input excitation current is 2 A, that is, when the ampere-turns

TABLE 4. Magnetic induction in the MRF channel under different current excitations.

excitation current	0. 5 A	1 A	1.5 A	2 A
magnetic induction intensity	0.1108 T	0.3768 T	0.6476 T	0.8285 T

FIGURE 15. Finger Tesla meter.

(a)

(b)   (c)

FIGURE 16. Test equipment: (a) dynamometer, (b) MR damper specific frock, and (c) MR damper on dynamometer.

number is 400, the magnetic induction intensity at the damping channel is 0.8285 T, which meets the design goal.

B. PERFORMANCE EXPERIMENT

The indicator machine is shown in Fig. 16 (a), the MR damper fully assembled was mounted onto the dynamometer, as illustrated in Fig. 16 (c). To extend the wires in the damper and connect them to the power source, a specific frock is utilized to link the damper and the top fixture, Fig. 16 (b) displays the installation fixture designed for the damper piston rod and wires. Currently, there is no industry-standard experiment specification for MR dampers. Therefore, the design of experiments for the MR damper was conducted by referencing the existing bench experiment method (QC/T 545-1999) used for ordinary dampers. The experiment stroke was set to 50 mm, and the experiment speeds were 0.052m/s, 0.131 m/s, 0.262 m/s, 0.393 m/s, and 0.52 m/s. Moreover, the experiment currents were 0 A, 0.5 A, 1 A, 1.5 A, and 2 A, respectively.

The test results of MR Shock absorber are organized into indicator curves, and the results are shown in Fig. 17. Most of the existing MR Dampers are single-channel structures and achieve asymmetric damping characteristics by adjusting the excitation current. This control method requires real-time control of the piston displacement and coil current of the damper. The force sensor is required to have high accuracy, and the current excitation control system has high efficiency and accuracy. Otherwise, when the piston runs at a fast speed, it is easy to cause an abrupt change of damping force, which is shown in the indicator diagram as sharp corners or depressions in the transition section of the recovery and compression stroke of the curve. At the same time, it will also enlarge the time-delay characteristics of the MRF itself, resulting in left and right asymmetry of the indicator curve about the S=0 line. As can be seen from Fig. 17, although there are slight fluctuations at the recovery and compression ends in
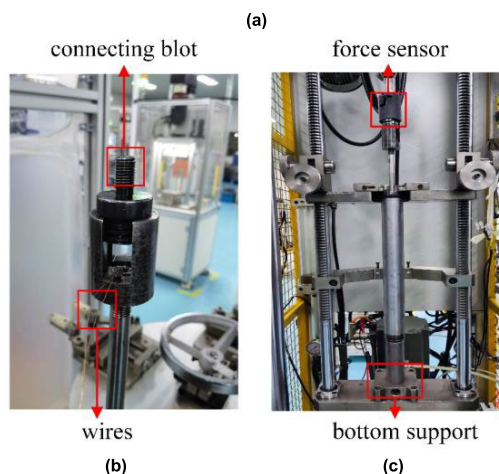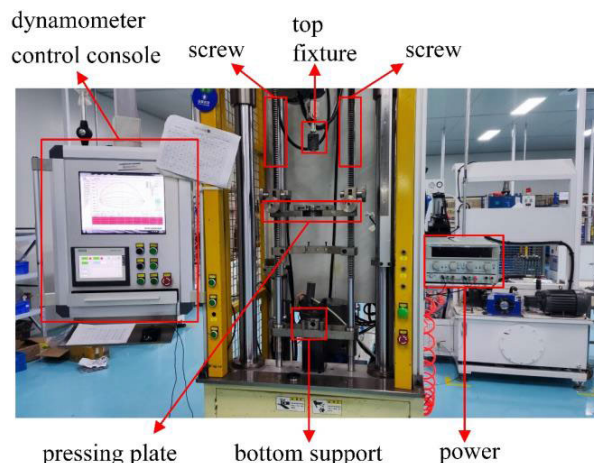
individual current cases, the indicator work curve is relatively smooth as a whole, without obvious depression, empty path, and impact. The indicator work curve is full, and the straight line symmetry about S = 0 is good. This shows that the MR Damper designed in this paper can realize the asymmetric damping characteristics of compression and recovery process without real-time control and effectively reduce the influence of MRF time delay. The cause of the fluctuation at the end of the recovery and compression stroke may be the abrupt change in the MRF flow rate during the opening and closing of the valve disc.

In the MR damper structure designed in this article, the valve plate and claw spring cooperate with each other to open the damping channel through the displacement of the valve plate. The speed and range of valve plate movement are related to the stiffness and height of the claw spring, while the claw spring has a lower stiffness and a shorter stroke. When the piston starts to move, the MRF pushes open the valve plate, and the valve plate at the outlet of the damping channel quickly changes from closed to fully open. The
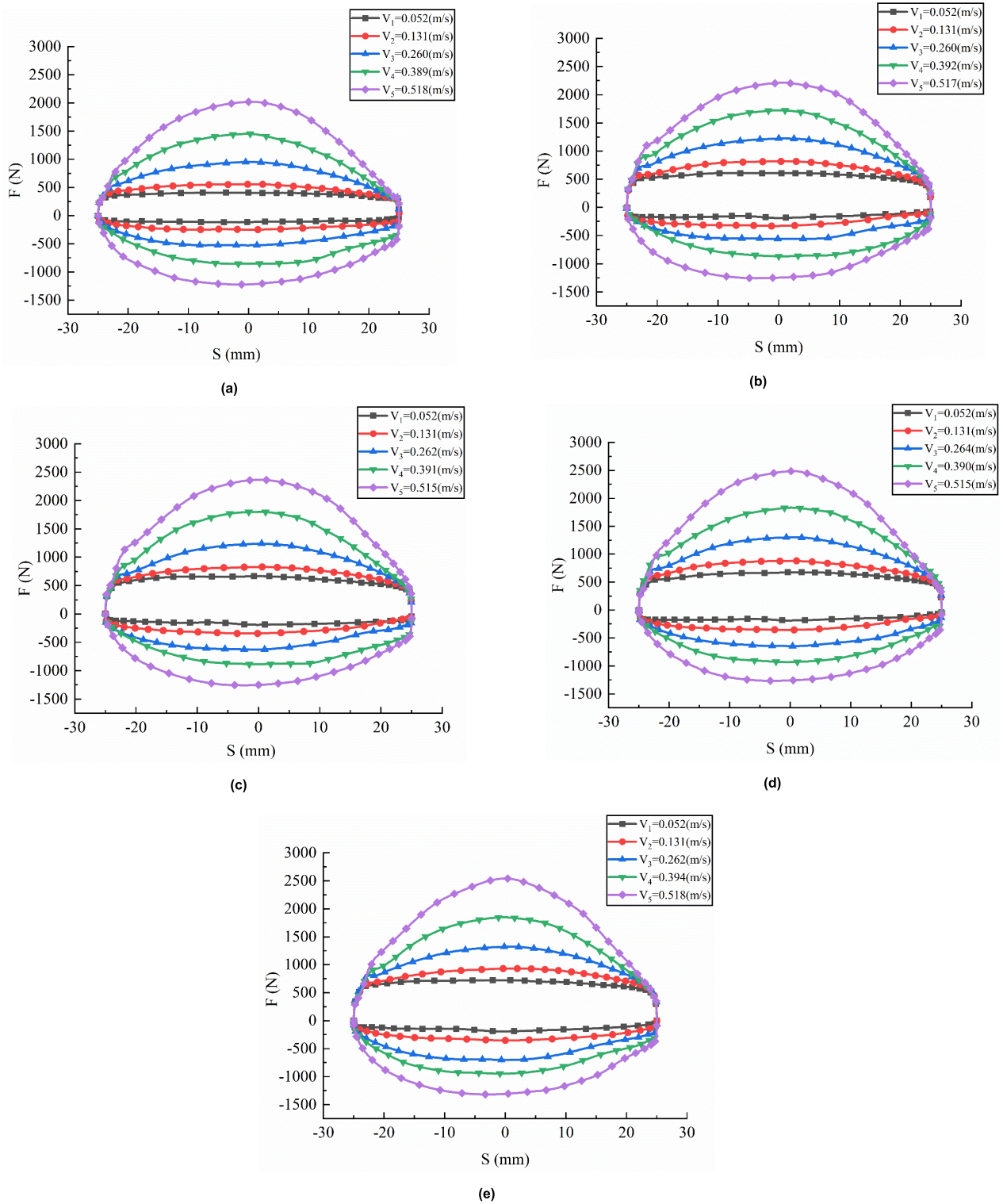
FIGURE 17. MR damper performance curve (a) I=0 A, (b) I=0.5 A, (c) I=1 A, (d) I=1.5 A, and (e) I=2 A.

damping fluid flow rate suddenly increases, and the damping force growth amplitude decreases. On the Fig. 17, it shows fluctuations at the left and right ends of the performance curve.

C. COMPARE EXPERIMENTAL RESULTS WITH DESIGN OBJECTIVES

The indicator curves under different current excitations with a piston motion speed of 0.52 m/s are shown in Fig. 18 (a). The
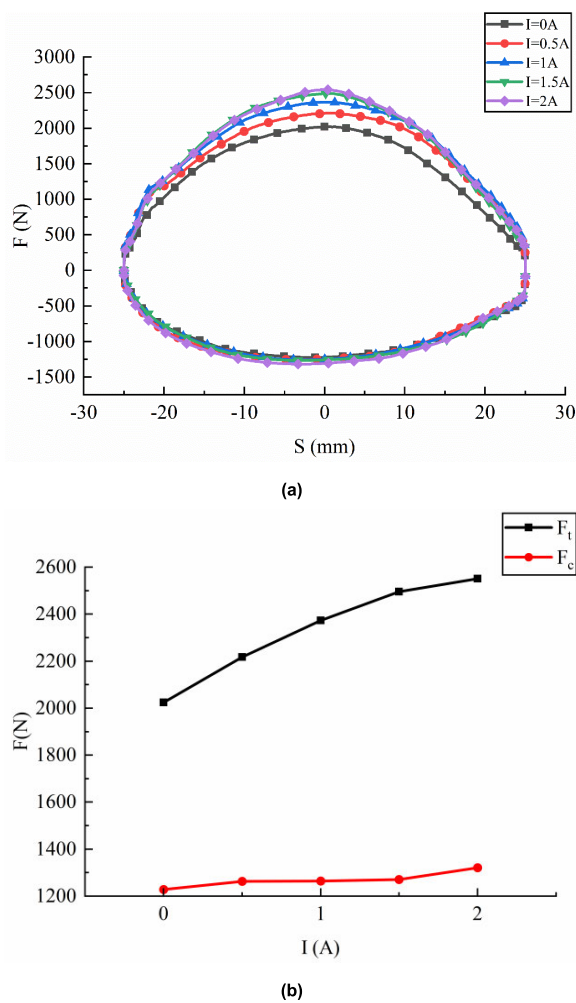
FIGURE 18. (a) Indicator curve at 0.52 m/s and (b) Summary of the maximum damping force.

maximum recovery and compression force values extracted from the curve are shown in Fig. 18 (b), where F_t represents the maximum recovery damping force and F_c represents the maximum compression damping force.

It can be seen from Fig. 18 that the maximum compression damping force at 0.52 m/s has little change with the change of current excitation, and the maximum recovery damping force increases with the increase of current excitation. When the current excitation is 0 A, the maximum recovery damping force is 2024.47 N, and the maximum zero-field compression damping force is 1228.05 N, which is in line with the design goal of 2000 N. The maximum zero field recovery damping force and the compression damping force are about 1/2 of the recovery damping force. When the current excitation is 2 A, the maximum recovery damping force is 2551.61 N, the damping force adjustment range is 527.13 N, the maximum compression damping force is 1320.65 N, and the damping force adjustment range is 92.6 N. This meets the design goal that the maximum recovery damping force adjustable range is not less than 500 N, and the maximum compression damping force changes little with the current excitation.

The adjustable range of the recovery damping force is 527.13 N, which is smaller than the theoretical calculation result of 636.54 N slightly. The possible reason is that during the experiment, the MRF distribution in the damping channel was uneven due to the arrangement of the electromagnetic coil in the middle of the piston body, and the heating of the electromagnetic coil after being energized caused a decrease in the MRF viscosity in the working cylinder, resulting in a decrease in the damping force of the damper.

VI. CONCLUSION

Aiming at the problems that the damping force is not high and the implementation process of asymmetric damping characteristics is complex in the current MR Damper, a structural improvement design of MR Damper was carried out. Through the combination of theoretical calculation and electromagnetic simulation, the key parameters and dimensions of the structure are determined, and the prototype is completed and tested. The experimental results show that the damper works well, and the designed damper can effectively reduce the influence of MRF time-delay.

The article presents the main research work and accomplishments as follows:

(1) Improvement of the structure of MR damper. A damper structure with asymmetric damping characteristics has been designed.

(2) Prototype production and experimentation. Based on the calculation of damping force and electromagnetic simulation, the dimensions of key components are determined, and a prototype is manufactured for conducting a demonstration of its power characteristic test.

(3) Summary of test results. The indicator curve is full and smooth, and the shock absorber works well. The indicator curve is smooth in the transition section of the recovery and compression stroke, without obvious sharp corners and depression. The symmetry of the straight line about S = 0 is good, and the damping force meets the proposed design goal.

However, the shock absorber designed in this paper still has some shortcomings, and future research can make some improvements:

(1) In the subsequent research, the structure of the damper can be optimized based on improving the adjustable range of damping force of the MR Damper, so that the damper has superior performance and a wider application range.

(2) The structural design, partial simulation, processing, and test of asymmetric damping structure MR Damper are carried out in this paper. However, the simulation analysis and test research are not in-depth enough. In the next step, more in-depth research can be carried out, and 1/4 vehicle or real vehicle verification is considered.

(3) When the MR Damper structure designed in this paper is assembled, the sealing situation at the hole where the wire is extended and the groove of the coil is complex, and there is no good sealing device. Although the existing ABS rubber

sealing method can meet the needs of short-term tests, its sealing strength is not high, and there is a risk of oil leakage in long-term use.

REFERENCES

[1] H. Jiang, "Performance simulation and testing of two-levels-damping adjustable hydraulic shock absorber," *J. Mech. Eng.*, vol. 46, no. 22, pp. 117–122, 2010.

[2] Y. Zhang, J. Guo, J. Yang, and X. Li, "Recent structural developments and applications of magnetorheological dampers (MRD): A review," *Magnetochemistry*, vol. 9, no. 4, pp. 90–97, Mar. 2023.

[3] J. D. Carlson, D. M. Catanzarite, and S. K. A. Clair, "Commercial magneto-rhelogical fluid devices," *Int. J. Mod. Phys. B*, vol. 10, nos. 23–24, pp. 48–57, Oct. 1996.

[4] L. Jiang, X. Yang, H. Liu, and Z. Li, "Design and experimental investigation of a novel twin-tube MR damper with meandering channel," *J. Magn. Magn. Mater.*, vol. 588, Dec. 2023, Art. no. 171443.

[5] A. Kumar Kariganaur, H. Kumar, and M. Arun, "Study on operational temperature of magneto-rheological fluid and design dimensions of magneto-rheological damper for optimization," *Eng. Res. Exp.*, vol. 6, no. 2, Jun. 2024, Art. no. 025510.

[6] M. E. H. Jamadar, P. Devikiran, R. M. Desai, H. Kumar, and S. Joladarashi, "Real-time testing and thermal characterization of a cost-effective magneto-rheological (MR) damper for four-wheeler application," *J. Brazilian Soc. Mech. Sci. Eng.*, vol. 45, no. 2, pp. 95–109, Jan. 2023.

[7] Y. Shiao and T.-L. Huynh, "Design and optimization of a new flow-mode magnetorheological mount with compact structure and extended workable force," *J. Intell. Mater. Syst. Struct.*, vol. 34, no. 20, pp. 2404–2413, Jul. 2023.

[8] J. Cao, D. Ning, P. Liu, S. Sun, G. Liu, and H. Du, "A versatile semi-active magnetorheological inerter with energy harvesting and active control capabilities," *Smart Mater. Struct.*, vol. 33, no. 1, Jan. 2024, Art. no. 015040.

[9] J. Yu, X. Dong, and Z. Zhang, "Design and control of a automobile novel magneto-rheological shock absorber with asymmetric mechanics properties," *China Mech. Eng.*, vol. 28, no. 3, pp. 372–377, Feb. 2017.

[10] C. Li, "The research of magnetorheological damper's time delay and control," M.S. thesis, College Mater. Sci. Eng., Chongqing Univ., Chongqing, China, 2010.

[11] R. L. L. G. Hidayat, Wibowo, B. Santoso, F. Imaddudin, and Ubaidillah, "Selection of MR damper model suitable for SMC applied to semi-active suspension system by using similarity measures," *Open Eng.*, vol. 12, no. 1, pp. 1005–1012, Dec. 2022.

[12] B. Sapiński, J. Gołdasz, Ł. Jastrzębski, M. Awtoniuk, and R. Sałat, "On the application of support vector method for predicting the current response of MR dampers control circuit," *Energies*, vol. 15, no. 24, pp. 9626–9641, Dec. 2022.

[13] L. Xie, C. Lu, J. Yin, B. Wei, Y. Wang, P. Wang, Z. Yang, and C. Liao, "A high-speed current source for magnetorheological applications," *Sci. Rep.*, vol. 13, no. 1, p. 17509, Oct. 2023.

[14] Y. Liu, X. Yang, D. Li, and G. Xie, "Study on the structural design and performance of magnetorheological (MR) valve with hybrid supply magnetic source and double annular channels," *J. Magn. Magn. Mater.*, vol. 570, Mar. 2023, Art. no. 170506.

[15] P. N. Vishwakarma, P. Mishra, and S. K. Sharma, "Characterization of a magnetorheological fluid damper a review," *Mater. Today, Proc.*, vol. 56, pp. 2988–2994, Jan. 2022.

[16] X. Hu, H. Zhou, F. Tu, W. Zhang, L. Wang, and S. Liu, "A high-speed vibration damper for rotary mixed magneto rheological fluid and its method for vortex mixing of magneto rheological fluid," CN Patent 2020 10 005 493, Mar. 12, 2021.

[17] Z. Deng, X. Wei, Q. Yang, Q. Cai, and S. Zhu, "Multi magnetic circuit magnetorheological shock absorber with permanent magnets," CN Patent 2019 11 146 531, Sep. 14, 2021.

[18] X. Liu, Y. Zhang, H. Hu, Z. Li, Z. Fu, B. Xu, X. Yao, Z. Dong, and Z. Wang, "A high-speed vibration damper for rotary mixed magneto rheological fluid and its method for vortex mixing of magneto rheological fluid," CN Patent 2021 10 576 557, Nov. 5, 2021.

[19] S. Zhu, P. Huang, D. Zhang, X. Zhou, and J. Yuan, "A new type of magneto rheological damper with piston inner flow channel," CN Patent 2017 10 306 815, Jul. 25, 2017.

[20] Y. Jia, "Design and experimental research on the vehicle twin-tube magnetorheological fluids damper based on pressure driven flow mode," *J. Mech. Eng.*, vol. 48, no. 10, pp. 103–108, May 2012.

[21] X. Zhu, X. Jing, and L. Cheng, "Magnetorheological fluid dampers: A review on structure design and analysis," *J. Intell. Mater. Syst. Struct.*, vol. 23, no. 8, pp. 839–873, Mar. 2012.

[22] J. W. Sohn, J.-S. Oh, and S.-B. Choi, "Design and novel type of a magnetorheological damper featuring piston bypass hole," *Smart Mater. Struct.*, vol. 24, no. 3, Feb. 2015, Art. no. 035013.

[23] G. T. Mata, "Characterization of dual annular duct MR damper with numerical and computational approach," *J. Vibrat. Eng. Technol.*, vol. 12, no. 3, pp. 3625–3640, Mar. 2024.

[24] M. Mao, W. Hu, Y.-T. Choi, N. M. Wereley, A. L. Browne, J. Ulicny, and N. Johnson, "Nonlinear modeling of magnetorheological energy absorbers under impact conditions," *Smart Mater. Struct.*, vol. 22, no. 11, Oct. 2013, Art. no. 115015.

[25] M. Mao, "Adaptive magnetorheological sliding seat system for ground vehicles," Ph.D. dissertation, Dept. Aerosp. Eng., Univ. Maryland, Baltimore, MD, USA, 2011.

[26] X. Wu, "Research on high power magnetorheological fluid stability transmission technology," Ph.D. dissertation, College Mechtron. Eng., China Univ. Mining Technol., Jiangsu, China, 2017.

JIANGQI LONG received the Ph.D. degree in automotive engineering from South China University of Technology, in 2009. He is currently working as a Professor with the College of Mechanical and Electrical Engineering, Wenzhou University. His research interests include the design of intelligent electronic controlled suspension systems for new energy vehicles and the lightweight design and manufacturing technology for auto-mobile and component structures.

MIN ZHOU was born in 1999. He received the B.S. degree in vehicle engineering from Hebei University of Science and Technology. He is currently pursuing the M.S. degree in mechanical and electrical engineering with Wenzhou University. His research interests include new energy vehicle drive and control and shock absorber structure design.

YINGHAO HU was born in 1996. He is currently pursuing the degree with the School of Mechanical and Electrical Engineering, Wenzhou University. His research interests include lightweight design of auto parts and analysis of stiffness characteristics of air spring and structural design of MR damper.

JIANHONG ZHANG is currently working as the Director of the Department of Technology Research and Development and the Technical Department, Anhui Sensen Intelligent Electronic Control Suspension System Company Ltd., and also with the Zhejiang Sensen Auto Parts Ltd. His research interests include the products design and development of automobile shock absorber solenoid valve, air spring, damper assembly, and other auto products.

• • •